Materials Horizons

ROYAL SOCIETY OF CHEMISTRY

COMMUNICATION

View Article Online
View Journal | View Issue

Cite this: *Mater. Horiz.*, 2025, **12**, 5204

Received 4th January 2025,
Accepted 11th April 2025

DOI: 10.1039/d5mh00011d

rsc.li/materials-horizons

Non-centrosymmetric structures designed rationally *via* a "dimensionality addition" strategy toward the promising nonlinear optical family [A–X][In–Se] (A = K/Ba and Rb/Ba; X = Cl and Br)†

Shao-Min Pei,[ab] Fan Wu,[a] Ming-Shu Zhang,[a] Wen-Fa Chen,[a] Xiao-Ming Jiang,[ab] Bin-Wen Liu *[ab] and Guo-Cong Guo *[ab]

Formulating a well-defined strategy for designing non-centrosymmetric (NCS) structures is an urgent requirement but a formidable challenge. Herein, we conducted a comprehensive statistical analysis of tetrahedra-based chalcogenide systems, revealing a significantly high probability for obtaining NCS structures in rigid three-dimensional (3D) systems, where the arrangement of tetrahedral units is minimally influenced by the non-directional spherical coordination of electropositive cations. Based on this premise, a "dimensionality addition" strategy implemented by regulating the A/M ratio (A = electropositive cations and M = tetrahedrally coordinated cations) is established for the first time. Consequently, six 3D NCS salt-inclusion selenides were successfully synthesized, namely, $A[A_4Cl][In_{14}Se_{23}]$ (A = K and Rb), $A_2[A_3BaCl][In_{18}Se_{30}]$ (A = K and Rb), and $[K_4Cl][AK_{9-10}Cl_4][In_{22}Se_{38}]$ (A = Li and Ba). All these compounds collectively employed separated polycations as "dimension regulators" to facilitate the assembly of $[InSe_4]$ tetrahedra into 3D NCS diamond-like frameworks, enabling promising second-harmonic generation (SHG) responses (0.69–2.10 × $AgGaS_2$). This study may serve as an instructive guidance for exploring symmetry-dependent materials.

New concepts

"Dimensionality addition" strategy implemented by regulating the A/M ratio is a brand-new concept for designing non-centrosymmetric (NCS) nonlinear optical (NLO) materials. A statistical analysis from the ICSD database indicated that the proportion of NCS $[MQ_4]$-based chalcogenides with a 3D framework is significantly higher than low-dimensional ones, with this trend being particularly pronounced in salt-inclusion chalcogenides (SICs). Inspired from these findings, we proposed a "dimensionality addition" strategy for synthesizing 3D SICs, employing a low A/In ratio to facilitate the aggregation of $[InSe_4]$ tetrahedra, thereby assembling well-ordered diamond-like frameworks. Six 3D NCS $[InSe_4]$-based SICs were successfully synthesized by controlling A/In ratios at low values, namely, $A[A_4Cl][In_{14}Se_{23}]$ (A = K and Rb), $A_2[A_3BaCl][In_{18}Se_{30}]$ (A = K and Rb), $[K_4Cl][LiK_{10}Cl_4][In_{22}Se_{38}]$, and $[K_4Cl][BaK_9Cl_4][In_{22}Se_{38}]$. All the compounds displayed robust second-harmonic generation responses, firmly validating the efficacy and applicability of the "dimensionality addition" strategy in the development of NCS structures and high-performance NLO materials.

Introduction

Non-centrosymmetric (NCS) crystalline materials possess numerous technologically crucial characteristics such as ferroelectricity,[1] piezoelectricity,[2] and particularly second-order nonlinear optical (NLO) effects, which play indispensable roles in laser therapy and laser guidance.[3] Given the inherent symmetry-dependence of NLO materials, a multitude of strategies have been developed to facilitate the controllable design of NCS structures, which can be broadly categorized into three as follows: (1) the deliberate selection and assembly of NLO-active structural modules, such as distorted tetrahedra, stereochemical-active lone pairs cations, and triangular plane groups, can greatly enhance the likelihood of acquiring NCS structure, such as $K_9[B_4O_5(OH)_4]_3(CO_3)(BO_2)$,[4] $Hg_7P_2Se_{12}$,[5] and $Cs_2YB_3O_6F_2$.[6,7] (2) Adopting template-involved structural modification approaches by incorporating asymmetric units or substituting redundant elements and motifs within centrosymmetric (CS) templates to disrupt the symmetry center, thereby enabling a CS-to-NCS transition,[8] or by substituting chemical counterparts in advantageous NCS templates to establish a transformation of NCS-to-NCS.[9] (3) Integrating advanced machine learning techniques to unveil the underlying NCS structures, such as leveraging first-principles calculations to screen potential NCS structures concealed in crystallographic databases or employing an *ab initio* evolutionary algorithm for predicting feasible NCS structures.[10] However, these strategies predominantly encounter the limitations of highly restricted research systems, necessitating the

[a] *State Key Laboratory of Structural Chemistry, Fujian Institute of Research on the Structure of Matter, Chinese Academy of Sciences, Fuzhou, Fujian 350002, People's Republic of China. E-mail: bwliu@fjirsm.ac.cn*

[b] *Fujian Science & Technology Innovation Laboratory for Optoelectronic Information of China, Fuzhou, Fujian 350002, People's Republic of China. E-mail: gcguo@fjirsm.ac.cn*

† Electronic supplementary information (ESI) available. CCDC 2371874, 2371875, 2371877, 2371878, 2371879 and 2371881. For ESI and crystallographic data in CIF or other electronic format see DOI: https://doi.org/10.1039/d5mh00011d

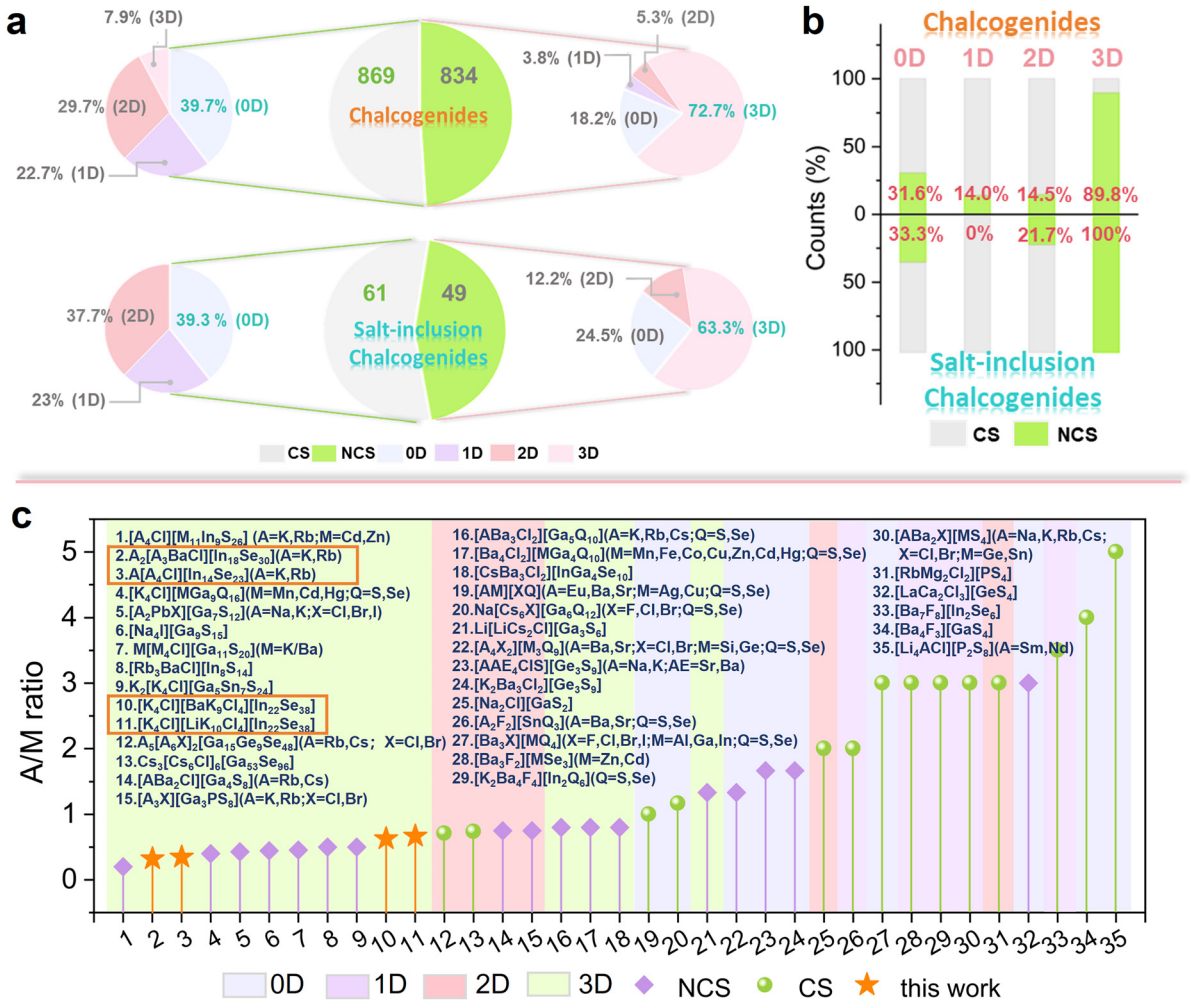

Fig. 1 Dimensional distribution of CS and NCS [MQ_4]-based chalcogenides and salt-inclusion chalcogenides (SICs) (a); proportion of NCS and CS structures of [MQ_4]-based chalcogenides and SICs in each dimension (b); and the relationship between A/M, structural symmetry and dimension of [MQ_4]-based SIC (c). (Note: the number of [MQ_4]-based chalcogenides and SICs are 1703 and 110, respectively; A represents electropositive cations and M represents tetrahedrally coordinated cations).

integration of more precisely defined and widely feasible strategies for designing ideal NCS compounds.

Revealing the inherent laws governing structural dimension and microscopic symmetry using statistical methods can provide empirical guidance for achieving optimal structures. Herein, we present a comprehensive overview of known [MQ_4]-based chalcogenide systems from the inorganic crystal structure database (ICSD), where M represents tetrahedrally coordinated cations and Q denotes S or Se. As depicted in Fig. 1, in NCS chalcogenides, the 3D structural framework has a definite predominance (72.7%); while in CS chalcogenides, the non-3D structure constitutes the dominant group (92.1%). From an alternative perspective, the majority of the 3D chalcogenides adopt NCS space groups, with only approximately 10.2% displaying CS structures (Fig. 1b). These findings indicate a preference for NCS space groups in the crystallization of 3D [MQ_4]-based chalcogenides, which can be attributed to the fact that 3D covalent frameworks composed of acentric tetrahedra exhibit relatively ordered tetrahedral polarization orientations and higher rigidity than non-3D frameworks, enabling them to resist the CS tendency caused by the non-directionality and non-saturation coordination characteristics of (poly)cations. Salt-inclusion chalcogenide (SIC) represents a significant subclass of chalcogenides. The incorporation of inorganic salt polycations effectively mitigates the common issue of the low laser-induced damage threshold (LIDT) associated with the narrow bandgap in conventional chalcogenides, positioning SICs as perfect NLO candidates for investigation. The statistical results of the SIC indicate that 3D structures remain the mainstay that makes up the NCS population. Of particular interest is that the NCS ratio of 3D SICs reaches 100%, representing a substantial improvement over the 89.9% observed for chalcogenides. The above statistical results demonstrate that employing the "dimensionality addition" strategy to construct a 3D rigid framework within SIC systems could be a highly efficient approach for attaining NCS structures.

For this purpose, we establish a correlation between the component ratio (A/M, where A represents electropositive

cations), structural symmetry and dimension of $[MQ_4]$-based SIC system to develop an experimentally available "dimensionality addition" strategy. As presented in Fig. 1c, when the A/M ratio is below 0.7, it tends to favor the adoption of a 3D structure, while when it exceeds 1.33, there is a propensity to adopt a non-3D structure. Essentially, employing a low A/M ratio can promote the facile aggregation of highly concentrated tetrahedra into rigid 3D frameworks with positive microscopic polarizability, thereby maximizing the probability of constructing an NCS structure. Drawing inspiration from the aforementioned findings, we adopted the "dimensionality addition" strategy achieved by systematically adjusting the A/In ratio, leading to the successful synthesis of six $[InSe_4]$-based SICs: $A[A_4Cl][In_{14}Se_{23}]$ (A = K **1**, Rb **2**), $A_2[A_3BaCl][In_{18}Se_{30}]$ (A = K **3**, Rb **4**), and $[K_4Cl][AK_{9-10}Cl_4][In_{22}Se_{38}]$ (A = Li **5**, Ba **6**). All these compounds utilize isolated polycations as "dimension regulators" to facilitate the assembly of the $[InSe_4]$ tetrahedra into NCS diamond-like frameworks, and such characteristics further demonstrate the reliability of our strategy. As anticipated, the outstanding NLO performances exhibited by compounds **1–6** demonstrated their promising potential as NLO candidates.

Results and discussion

Compounds **1–6** are configured by vertex-shared $[InSe_4]$ tetrahedra, which ultimately present similar diamond-like frameworks carrying negative charges and abundant vacancies, and the vacancy-formed channels are evenly packed with polycations to sustain charge neutrality (Fig. 2a). The intrinsic relationships between these compounds and their distinctions from those In-based SICs are further elaborated later in this section. Detailed crystal structures represented by compounds **1**, **3**, and **5** are illustrated in Fig. 2. The ortep plots of compounds **1–6** are shown in Fig. S1 (ESI†). Crystallographic parameters, relevant atom coordinates and extracted bond lengths of **1–6** are displayed in Tables S1, S2 and S3 (ESI†), respectively. The energy-dispersive X-ray spectroscopy (EDS) analysis basically validated the correctness of formula **1–6** (Fig. S2, ESI†).

$K[K_4Cl][In_{14}Se_{23}]$ (1)

One of the fundamental layers of compound **1** is densely packed with $[In_{14}Se_{23}]$ T2-supertetrahedral clusters (Fig. 2c). Each cluster consists of two identical $[In_7Se_{16}]$ units arranged in different orientations. These $[In_7Se_{16}]$ units consist of two T2-supertetrahedra that share a common $[InSe_4]$ tetrahedra (Fig. 2d). The $[K_4Cl]^{3+}$ polycations and K^+ cations are strategically positioned to occupy the vacant spaces that correspond to their respective dimensions (Fig. 2b).

$K_2[K_3BaCl][In_{18}Se_{30}]$ (3)

The diamond-like anionic framework of compound **3** can be perceived as being constructed by layers A and B superimposed along the *c*-axis in an ABAB fashion (Fig. 2f). From a top-down perspective, layer A is formed by planar $[In_3Se_9]$ trimers

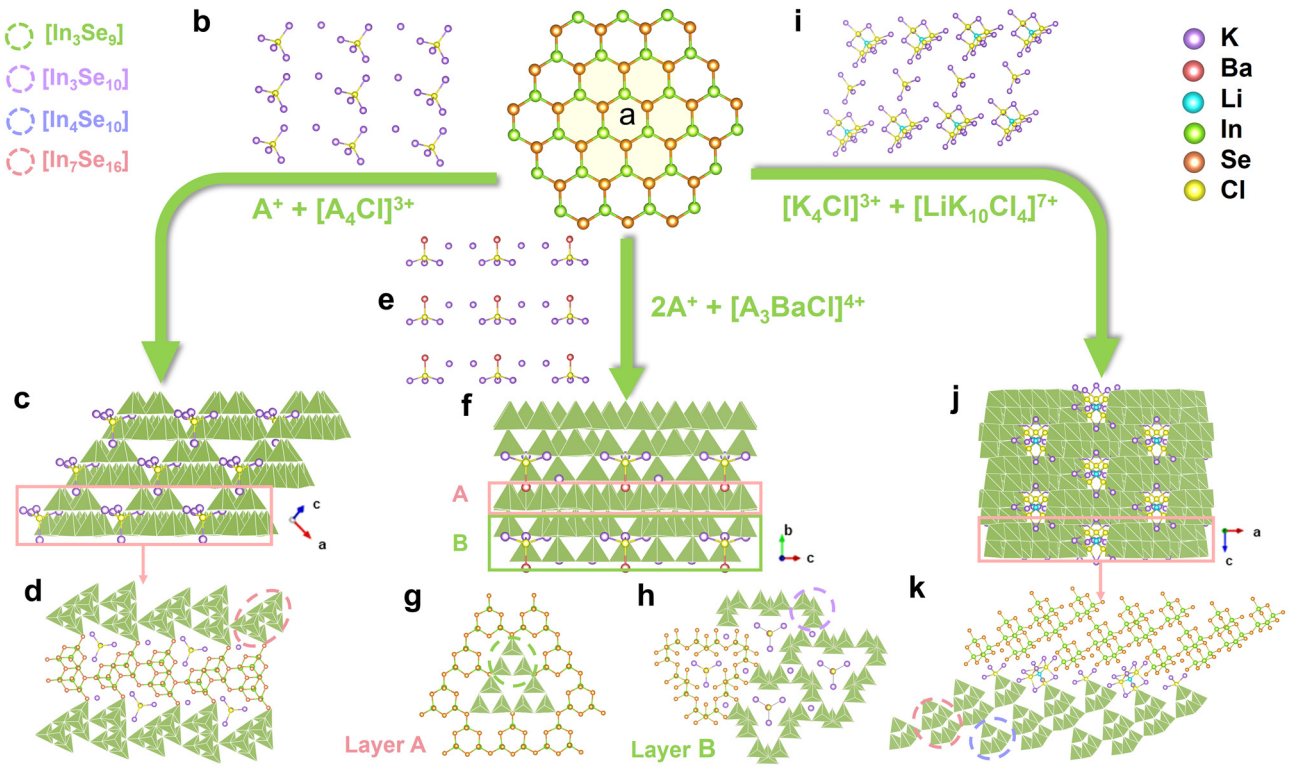

Fig. 2 An elementary $[InSe_4]$-based diamond-like framework (a); 3D crystal structure diagrams of **1** (c), **3** (f), and **5** (j); ball-and-stick models depicting the arrangement of cations or polycations in **1** (b), **3** (e), and **5** (i); basic repeating layers of **1** (d), **3** (g, h), and **5** (k).

interconnected by shared Se atoms (Fig. 2g), while layer B consists of recurring V-shaped $[In_3Se_{10}]$ trimers, with six such trimers linked head to tail to create a triangular-like six-membered ring filled with $[K_3BaCl]^{4+}$ polycations, and K^+ ions are distributed within small cavities around the periphery of the six-membered ring (Fig. 2e and h).

$[K_4Cl][LiK_{10}Cl_4][In_{22}Se_{38}]$ (5)

The diamond-like framework of compound **5** involves two characteristic constituent units: $[In_4Se_{10}]$ T2-supertetrahedra, which is formed by sharing S-vertices among four $[InSe_4]$ tetrahedra, and $[In_7Se_{16}]$ tetrahedral cluster, which is created through two $[In_4Se_{10}]$ by co-occupying an adjoining $[InSe_4]$ tetrahedra. These two components are arranged in an ABBA configuration to produce a tetrahedral chain, which is further extended into a repeating layer of the diamond-like framework by employing Se atoms as connectors (Fig. 2j and k). In contrast to the prevailing single-guest SICs, compound **5** exhibits a unique feature of dual polycations, namely $[K_4Cl]^{3+}$ and $[LiK_{10}Cl_4]^{7+}$, which are precisely arranged within dimensionally matched cavities of the anion framework (Fig. 2i). The anionic framework of **6** is mirror-symmetric to that of **5**. In addition to identical $[K_4Cl]^{3+}$, they also share resemblant polycations, namely $[LiK_{10}Cl_4]^{7+}$ and $[BaK_9Cl_4]^{7+}$, which can be interconverted by aliovalent substitution. As depicted in Fig. S3 (ESI†), Li^+ ion is observed to occupy the center of T2-supertetrahedra in the absence of Ba^{2+} owing to its tiny size and ability to compensate for the charge deficiency. This structural transformation offers a viable solution for the eradication of disordered defects.

Based on the aforementioned structural analysis, we present a diagrammatic representation illustrating the internal relationships among these four types of $[InSe_4]$-based SICs (Fig. 3a). Obviously, the varying concentrations of $[InSe_4]$ and the presence of diverse cations or/and polycations give rise to their multiform structures. As additional $[InSe_4]$ tetrahedra are incorporated, the anionic frameworks become increasingly negatively charged. In such cases, the introduction or substitution of higher-charged cations or polycations, such as Ba^{2+} and $[K_4Cl]^{3+}$, can facilitate the attainment of electrical neutrality. Furthermore, we attempted to sort out the potential correlation between the A/M ratio as well as the structural dimension and symmetry. According to our conclusion, the primary factor driving the preference of certain $[MQ_4]$-based SICs for CS space groups is their elevated A/M ratio. In truth, highly concentrated alkali or alkaline-earth metals connected by halogens can bind in a large-span spatial configuration, and A–Q ionic bonds are widely recognized as non-directional and non-saturated. Those structures with cations or/and polycations as protagonists mostly tend to adopt nearly "sphere" coordination, resulting in a flexible and low-dimensional (0D, 1D or 2D) anionic framework whose $[MQ_4]$ tetrahedra display promiscuous and counteracting polarization directions (Fig. 3b).[11] These structural features always exhibit a CS crystalline nature. Conversely, in the case of a low A/M ratio, asymmetric $[MQ_4]$ tetrahedra tend to aggregate and yield rigid high-dimensional frameworks

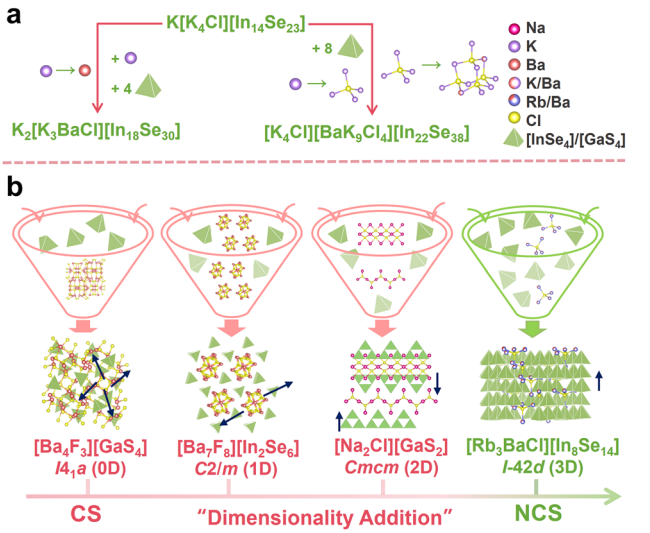

Fig. 3 Schematic of the internal transformation occurring among compounds **1**, **3**, and **6** (a); diagram illustrating the process of the "dimensionality addition" strategy (b). Note: the navy-blue arrows in (b) represent the polarization direction of the tetrahedra.

with a uniform microscopic polarization direction, which ultimately combine with low-concentration cation or polycation to assemble ideal NCS structures.[12] Therefore, taking advantage of the "dimensionality addition" strategy of regulating the A/M ratio to yield a 3D rigid framework can significantly enhance the likelihood of obtaining the NCS structures. From the "dimensionality reduction" perspective, the dimension of the anionic framework is largely governed by polycation; in other words, polycation functions as a "dimension regulator".[13] As presented by the title compounds, the isolated polycations show a preference for matching the promising NCS diamond-like framework. The identification of these structural correlations offers valuable insights for the screening and design of symmetry-dependent structures.

The purities of the polycrystalline powder of compounds **1–6** were validated by XRD analyses (Fig. S4, ESI†). A perfect agreement between the experimental and simulated patterns fitted from single-crystal XRD suggests that all the polycrystalline samples employed for subsequent measurements are pure phases. In view of the NCS crystallization of **1–6**, it is pertinent to investigate their double frequency conversion efficiencies. Their powder SHG efficiencies were assessed based on the Kurtz–Perry method under 1910 nm laser irradiation, with commercially acquired $AgGaS_2$ (AGS) serving as a standard sample.[14] The SHG intensities of strictly screened crystals **1–6** and AGS were evaluated within five particle size ranges (30–50, 50–75, 75–100, 100–150, and 150–200 μm). It was obvious that the SHG intensities of compounds **5**, **6** and AGS demonstrated a consistent growth trend in relation to particle sizes, indicating their phase-matching behaviors, while these trends were absent in compounds **1–4**, revealing non-phase-matching capabilities (Fig. 4a). The comparison of SHG intensities at a particle size range of 150–200 μm is illustrated in Fig. 4b, and the SHG intensities of **1–6** were observed to be

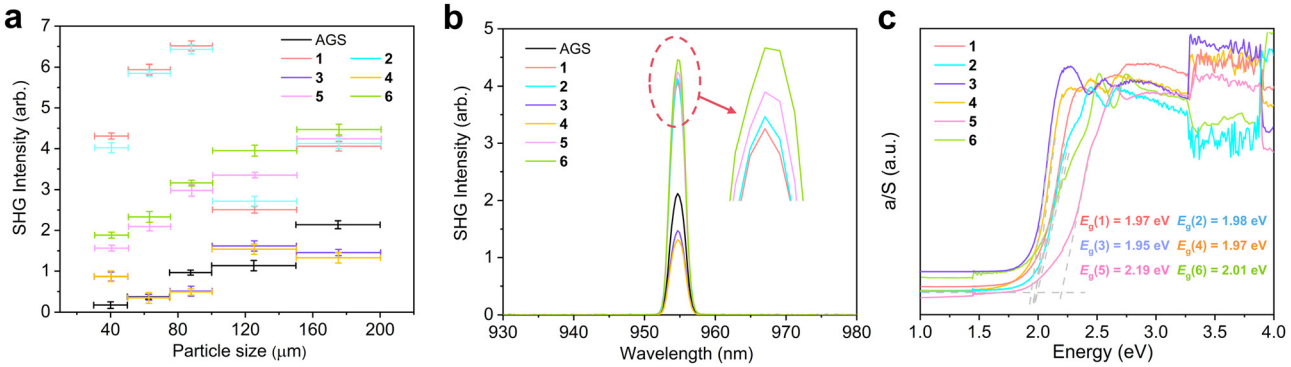

Fig. 4 (a) Particle-size dependence of SHG intensities of **1–6** and AGS. (b) SHG intensities of **1–6** and AGS within the particle size range of 150–200 μm under a 1910 nm radiation. (c) UV-Vis-NIR absorption spectra of **1–6**.

about 1.92, 1.95, 0.69, 0.62, 2.00, and 2.10 times those of the AGS. The relationship between the SHG intensity ($I^{2\omega}$) and effective NLO tensors (d_{eff}) can be described by $d_{eff} = d_{eff,AGS}\ (I^{2\omega}/I^{2\omega}_{AGS})^{1/2}$ (where $d_{eff,AGS}$ is equal to 11.6 pm V^{-1}), provided that the phase-matching requirements are met.[15] Based on this equation, the experimental d_{eff} of compounds **5** and **6** were confirmed to be 16.40 and 16.81 pm V^{-1}, respectively. These measured phase-matching SHG intensities are superior to those of most of the [GaS_4]-based SICs, including $Li[LiCs_2Cl][Ga_3S_6]$ (0.7 × AGS),[16] $[ABa_2Cl][Ga_4S_8]$ (A = Rb, Cs) (0.9–1.0 × AGS),[8c] $[K_3Cl][Mn_2Ga_6S_{12}]$ (0.8 × AGS),[17] $K_3Rb_3[K_3Cl][Li_2Mn_4Ga_{12}S_{27}]$ (1.1 × AGS);[9a] and commensurate with $[K_4Cl][CdGa_9Se_{16}]$ (2.4 × AGS),[18] and $[Rb_3BaCl][In_8Se_{14}]$ (2.0 × AGS),[12] but inferior to those of $[K_2PbX][Ga_7S_{12}]$ (X = Cl, Br and I) (Table S4, ESI†).[19]

Polycrystalline infrared spectra of **1–6** revealed no significant absorption peaks in the range of 2.5–25.0 μm (Fig. S5, ESI†), indicating their potential availability in the infrared region. LIDT is one of the most essential criteria for evaluating NLO materials. The mechanisms of damage caused by high-energy lasers are intricate, necessitating a comprehensive analysis of LIDT from multiple perspectives. Typically, the damage inflicted on crystal materials by nanosecond lasers consists primarily of dielectric breakdown and thermal damage, which can be mainly quantified as the optical bandgap and thermal expansion coefficient (TEC), respectively. Wide-bandgap materials, owing to their higher electric field strength and photon energy requirements for initiating electronic transitions, exhibit greater resistance to dielectric breakdown. This means that wide-bandgap materials are more capable of withstanding structural damage induced by high-energy lasers. The experimental bandgaps of **1–6** were finalized using the UV-Vis-NIR diffuse reflectance spectrum. By plotting F(R) *vs.* $h\nu$, the bandgaps of **1–6** were determined as 1.97, 1.98, 1.95, 1.97, 2.19, and 2.01 eV, respectively (Fig. 4c), which are superior to that of commercial $AgGaSe_2$ (1.82 eV), as well as those of salt-inclusion selenides, *e.g.*, $[Na_2Ba_{17}F_{18}][In_8Se_{21}]$ (1.73 eV),[11c] $[KBa_2F_2][InSe_3]$ (1.76 eV),[11c] $[K_3I][InB_{12}(InSe_4)_3]$ (1.97 eV),[20] $[Ba_3X][GaSe_4]$ (X = Cl and Br) (1.8–2.0 eV),[11a] and $[K_4Cl][CdGa_9Se_{16}]$ (1.72 eV).[18] The bandgap order of the title compounds follows the trend E_g (**5**, **6**) > E_g (**3**, **4**) ≈ E_g (**1**, **2**), demonstrating a direct proportionality to their corresponding A/In ratio. In addition, the experimental bandgap of 1.82 eV for γ-In_2Se_3 (the case of A = 0) is narrower than those of all the title SICs.[21] These observations suggest that increasing the concentration of cations or polycations can effectively enlarge the bandgap. The TECs (α) can be extrapolated from the temperature-dependent curves of the lattice parameters, reflecting the stability of the crystal lattice in response to thermal stimulation. Sixteen sets of cell parameters (20 K per step) were collected by applying a single-crystal XRD diffractometer in the temperature range of 100–400 K (Fig. S6, ESI†). The TEC values of **1–6** were determined using the formula $\alpha_L = \Delta L/L\Delta T$, where $\Delta L/\Delta T$ represents the slope obtained through linear regression analysis and L denotes the lattice constant at T = 100 K. The TECs of a, b, and c for **1–6** are listed in Table S5 (ESI†), and these results are significantly smaller than those of AGS. The LIDT results demonstrated that compounds **1–6** exhibited superior values compared to AGS, being 4.1, 3.6, 3.4, 3.1, 4.3, and 3.9 times higher than those of AGS, respectively (Table S6, ESI†). These enhancements may be attributed to the synergistic effect of appropriate bandgaps and lower TEC values.[22]

The electronic structures of **1–6** were computed to establish a comprehensive understanding of the profound relationship between structure and property.[23] The band structures performed using the CASTEP module indicate that **1–2** possessed the characteristics of indirect bandgap materials, with theoretical bandgap values of 1.55 and 1.56 eV, respectively, while **3–6** were identified as direct bandgap semiconductors, with bandgap values of 1.48, 1.42, 1.34, and 1.23 eV (Fig. S7, ESI†). All the theoretical bandgaps are smaller than the experimental results. The primary reason for the underestimation of the bandgap lies in the discontinuity of the wave function between the valence band maximum (VBM) and the conduction band minimum (CBM). The partial density of states (PDOS) analysis of **1–6** revealed a concentrated distribution of Se-p, Se-s, In-s, and In-p electronic states in the VBM, while the CBM was predominantly occupied by Se-p, In-p, and Cl-p electronic states with a minor contribution from Se-s states (Fig. 5a, b, and Fig. S8, ESI†). The overlap of In-p and Se-p orbitals ranging from −3 to 0 eV in **1–6** signified the formation of a chemical bond between the In and Se atoms. Additionally, compounds **5** and **6** were chosen as representatives to gain insights into their bonding character by calculating electron density difference (EDD) and crystal orbital

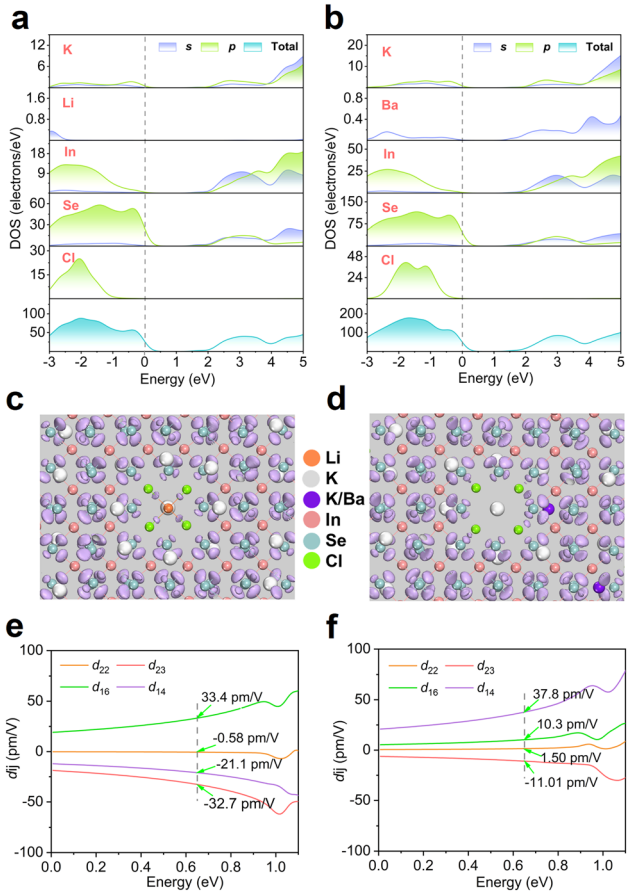

Fig. 5 Density of states (DOS) of **5** (a) and **6** (b); three-dimensional EDD diagram of **5** (c) and **6** (d) (isovalue is equal to 0.5); calculated frequency-dependent SHG tensors of **5** (e) and **6** (f).

Hamilton population (COHP).[24] As depicted in Fig. 5c and d, the electron aggregation between In and Se atoms, as well as Li and Cl atoms, could be observed in the EDD of compound **5**, demonstrating the presence of In–Se and Li–Cl covalent bonds. The COHP curves depicted in Fig. S9 (ESI†) illustrate the pronounced bonding character of In–Se pairs in **5** and **6**, and the Li–Cl pairs in **5** also demonstrate the characteristics of a weak covalent bond. The calculated ICOHP values for In–Se in **5** and **6** were −4.05175 and −4.11432, respectively, indicating stronger In–Se covalent bonds in **6** compared to **5**. The above analysis demonstrates that the outstanding SHG responses of **5** and **6** can primarily be attributed to their strong covalent $[InSe_4]$-based diamond-like frameworks. This inference is equally applicable to other title compounds.

The theoretical NLO coefficients were investigated using the ABINIT package based on density functional theory (DFT).[25] Adhering to the constraint of Kleiman Symmetry rule, the $P1$ space group adopted by **1** and **2** shows ten independent non-zero NLO tensors (d_{ij}), specifically d_{33}, d_{34}, d_{32}, d_{35}, d_{36}, d_{31}, d_{22}, d_{26}, d_{16}, and d_{14}; the $P6_3cm$ adopted by **3** and **4** demonstrates two non-zero d_{ij}, namely d_{31} and d_{33}; and the C_2 adopted by **5** and **6** encompasses four d_{ij}, specifically d_{22}, d_{23}, d_{16}, and d_{14}. As illustrated in Fig. S10a (ESI†), at a wavelength of 1910 nm (0.65 eV), the calculated d_{33}, d_{34}, d_{32}, d_{35}, d_{36}, d_{31}, d_{22}, d_{26}, d_{16}, and d_{14} for **1** were determined as −15.4, −18.2, 23.7, −24.0, −38.7, −7.5, −11.4, 8.0, 25.8, and 12.9 pm V^{-1}; and −14.4, −18.7, 24.0, −24.0, −39.7, −7.6, −11.8, 9.3, 26.6, and 13.6 pm V^{-1} for **2**, respectively. Similarly, the theoretical values of d_{31} and d_{33} were calculated as 16.7 and −19.4 for **3** and 16.3 and −19.6 for **4**, respectively (Fig. S10b, ESI†). The calculated d_{22}, d_{23}, d_{16}, and d_{14} for **5** were 33.4, −0.58, −21.1, and −32.7 pm V^{-1}; and 37.8, 10.3, 1.5, and −11.01 pm V^{-1} for **6**, respectively (Fig. 5e and f). These theoretical d_{ij} values of **1–6** aligned remarkably with the experimental values obtained earlier. These crystals exhibit significant SHG coefficients, high LIDTs, broad transmission spectra, and blocky crystal features, making them one of the top contenders in the field.

Conclusions

In light of the imperative and formidable task of designing NCS structures, the present study proposes a "dimensionality addition" strategy to achieve 3D rigid structures by adopting appropriate A/M ratios, thereby significantly increasing the possibility of attaining an NCS structure. Through the successful implementation of this strategy, six NCS SICs with diamond-like frameworks were produced, namely $A[A_4Cl][In_{14}Se_{23}]$ (A = K **1**, Rb **2**), $A_2[A_3BaCl][In_{18}Se_{30}]$ (A = K **3** and Rb **4**), and $[K_4Cl][AK_{9\sim10}Cl_4][In_{22}Se_{38}]$ (A = Li **5** and Ba **6**). The potentials of all compounds as excellent infrared NLO materials are demonstrated, supported by compelling evidence, including their robust SHG responses (0.69–2.1 × AGS @1910 nm) and decent bandgaps (∼2.0 eV). This creative work demonstrates the potential possibilities of tetrahedra-based SICs as infrared NLO materials, and the involved structural design concepts will ignite fresh inspiration for developing NCS structures essential for NLO materials.

Author contributions

S.-M. P.; B.-W. L.; and G.-C. G. conceived the project. S.-M. P.; and F. W. designed and carried out the experiments. X.-M. J.; M.-S. Z.; and W.-F. C. carried out the calculations. S.-M. P.; B.-W. L.; and G.-C. G. wrote and revised the manuscript.

Data availability

Crystallographic data for compounds **1–6** have been deposited at the ICSD under 2371874, 2371875, 2371878, 2371877, 2371881, and 2371879, respectively, and can be obtained from https://doi.org/10.1039/d5mh00011d.

Conflicts of interest

The authors declare no competing financial interests.

Acknowledgements

This work was supported by the National Natural Science Foundation of China (U21A20508, 22175172), the Youth Innovation Promotion Association of Chinese Academy of Sciences (2021300), Postdoctoral Fellowship Program of FPSF (GZC20232667), Fujian Science & Technology Innovation Laboratory for Optoelectronic Information of China (2020ZZ108) and Self-deployment Project Research Program of Haixi Institutes, Chinese Academy of Sciences (CXZX-2022-GH06).

References

1 I. Grinberg, D. V. West, M. Torres, G. Gou, D. M. Stein, L. Wu, G. Chen, E. M. Gallo, A. R. Akbashev, P. K. Davies, J. E. Spanier and A. M. Rappe, *Nature*, 2013, **503**, 509–512.

2 X.-M. Jiang, M.-J. Zhang, H.-Y. Zeng, G.-C. Guo and J.-S. Huang, *J. Am. Chem. Soc.*, 2011, **133**, 3410–3418.

3 (*a*) W. Zhou and S.-P. Guo, *Acc. Chem. Res.*, 2024, **57**, 648–660; (*b*) Y. Zhang, J. Chen, K. Li, H. Wu, Z. Hu, J. Wang, Y. Wu and H. Yu, *Nat. Commun.*, 2024, **15**, 2959; (*c*) M. Mutailipu, J. Han, Z. Li, F. Li, J. Li, F. Zhang, X. Long, Z. Yang and S. Pan, *Nat. Photonics*, 2023, **17**, 694–701; (*d*) H. Zhang, X. Jiang, Y. Zhang, K. Duanmu, C. Wu, Z. Lin, J. Xu, J. Yang, Z. Huang, M. G. Humphrey and C. Zhang, *J. Am. Chem. Soc.*, 2024, **146**, 28329–28338; (*e*) J. Wu, Y. Guo, J.-L. Qi, W.-D. Yao, S.-X. Yu, W. Liu and S.-P. Guo, *Angew. Chem., Int. Ed.*, 2023, **62**, e202301937; (*f*) Y. Tian, W. Zeng, X. Dong, L. Huang, Y. Zhou, H. Zeng, Z. Lin and G. Zou, *Angew. Chem., Int. Ed.*, 2024, **63**, e202409093; (*g*) Z. Bai and K. M. Ok, *Chem. Rev.*, 2023, **490**, 215212.

4 S. Liu, X. Jiang, L. Qi, Y. Hu, K. Duanmu, C. Wu, Z. Lin, Z. Huang, M. G. Humphrey and C. Zhang, *Angew. Chem., Int. Ed.*, 2024, **63**, e202403328.

5 Y. Chu, H. Wang, Q. Chen, X. Su, Z. Chen, Z. Yang, J. Li and S. Pan, *Adv. Funct. Mater.*, 2024, **34**, 2314933.

6 H. Wu, Z. Wei, Z. Hu, J. Wang, Y. Wu and H. Yu, *Angew. Chem., Int. Ed.*, 2024, **63**, e202406318.

7 (*a*) L. Luo, L. Wang, J. Chen, J. Zhou, Z. Yang, S. Pan and J. Li, *J. Am. Chem. Soc.*, 2022, **144**, 21916–21925; (*b*) X. Wang, X. Leng, Y. Kuk, J. Lee, Q. Jing and K. M. Ok, *Angew. Chem., Int. Ed.*, 2023, **63**, e202315434; (*c*) X. Wang, Y. Li, Z. Chen, J. Lee, F. Zhang, K. R. Poeppelmeier, S. Pan and K. M. Ok, *Small Struct*, 2023, **4**, 2300274.

8 (*a*) X.-H. Li, Z.-H. Shi, M. Yang, W. Liu and S.-P. Guo, *Angew. Chem., Int. Ed.*, 2022, **61**, e202115871; (*b*) J. Wang, H. Wu, H. Yu, Z. Hu, J. Wang and Y. Wu, *Adv. Opt. Mater.*, 2022, **10**, 2102673; (*c*) Z.-X. Qiu, Z.-X. Zheng, X.-M. Jiang, B.-W. Liu and G.-C. Guo, *Chem. Sci.*, 2023, **14**, 13568–13573; (*d*) B.-W. Liu, X.-M. Jiang, H.-Y. Zeng and G.-C. Guo, *J. Am. Chem. Soc.*, 2020, **142**, 10641–10645.

9 (*a*) S.-M. Pei, B.-W. Liu, W.-F. Chen, X.-M. Jiang and G.-C. Guo, *Mater. Horiz.*, 2023, **10**, 2921–2926; (*b*) L. Wu, C. Lin, H. Tian, Y. Zhou, H. Fan, S. Yang, N. Ye and M. Luo, *Angew. Chem., Int. Ed.*, 2024, **63**, e202315647; (*c*) J. Chen, H. Chen, F. Xu, L. Cao, X. Jiang, S. Yang, Y. Sun, X. Zhao, C. Lin and N. Ye, *J. Am. Chem. Soc.*, 2021, **143**, 10309–10316.

10 (*a*) M. Wu, E. Tikhonov, A. Tudi, I. Kruglov, X. Hou, C. Xie, S. Pan and Z. Yang, *Adv. Mater.*, 2023, **35**, 2300848; (*b*) Q. Wu, L. Kang and Z. Lin, *Adv. Mater.*, 2024, **36**, 2309675; (*c*) Y. Huang, D. Chu, Y. Zhang, C. Xie, G. Li and S. Pan, *Angew. Chem., Int. Ed.*, 2024, **63**, e202406576.

11 (*a*) K. Feng, W. Yin, Z. Lin, J. Yao and Y. Wu, *Inorg. Chem.*, 2013, **52**, 11503–11508; (*b*) X. Li, F. Liang, T. Liu and H. Li, *Dalton Trans.*, 2021, **50**, 11167–11172; (*c*) D. Gao, X. Ji, H. Yu, Z. Hu, J. Wang, Y. Wu and H. Wu, *J. Alloys Compd.*, 2023, **936**, 168141.

12 F. Wu, W.-F. Chen, Z.-X. Wu, X.-M. Jiang, B.-W. Liu and G.-C. Guo, *Sci. China Mater.*, 2024, **67**, 2000–2007.

13 J. Androulakis, S. C. Peter, H. Li, C. D. Malliakas, J. A. Peters, Z. Liu, B. W. Wessels, J. H. Song, H. Jin, A. J. Freeman and M. G. Kanatzidis, *Adv. Mater.*, 2011, **23**, 4163–4167.

14 S. K. Kurtz and T. T. Perry, *J. Appl. Phys.*, 1968, **39**, 3798–3813.

15 B.-W. Liu, H.-Y. Zeng, X.-M. Jiang and G.-C. Guo, *CCS Chem.*, 2020, **3**, 964–973.

16 B.-W. Liu, X.-M. Jiang, B.-X. Li, H.-Y. Zeng and G.-C. Guo, *Angew. Chem., Int. Ed.*, 2020, **59**, 4856–4859.

17 B.-W. Liu, S.-M. Pei, X.-M. Jiang and G.-C. Guo, *Mater. Horiz.*, 2022, **9**, 1513–1517.

18 S.-M. Pei, B.-W. Liu, X.-M. Jiang, Y.-Q. Zou, W.-F. Chen, Q.-N. Yan and G.-C. Guo, *Chem. Mater.*, 2021, **33**, 8831–8837.

19 W.-F. Chen, B.-W. Liu, S.-M. Pei, X.-M. Jiang and G.-C. Guo, *Adv. Sci.*, 2023, **10**, 2207630.

20 S.-S. Han, W.-D. Yao, S.-X. Yu, Y. Sun, A. Gong and S.-P. Guo, *Inorg. Chem.*, 2021, **60**, 3375–3383.

21 Y. Chi, Z.-D. Sun, Q.-T. Xu, H.-G. Xue and S.-P. Guo, *ACS Appl. Mater. Interfaces*, 2020, **12**, 17699–17705.

22 S.-F. Li, X.-M. Jiang, B.-W. Liu, D. Yan, C.-S. Lin, H.-Y. Zeng and G.-C. Guo, *Chem. Mater.*, 2017, **29**, 1796–1804.

23 (*a*) S. J. Clark, M. D. Segall, C. J. Pickard, P. J. Hasnip, M. J. Probert, K. Z. Refson and M. C. Payne, *Z. Kristallogr. Cryst. Mater*, 2005, **220**, 567–570; (*b*) X. Gonze, B. Amadon. and G. Antonius, *et al.*, *Comput. Phys. Commun.*, 2019, **248**, 107042.

24 R. Nelson, C. Ertural, J. George, V. L. Deringer, G. Hautier and R. Dronskowski, *J. Comput. Chem.*, 2020, **41**, 1931–1940.

25 (*a*) J. P. Perdew, J. A. Chevary, S. H. Vosko, K. A. Jackson, M. R. Pederson, D. J. Singh and C. Fiolhais, *Phys. Rev. B: Condens. Matter Mater. Phys.*, 1992, **46**, 6671–6687; (*b*) S. Baroni, S. Gironcoli, A. D. Corso and P. Giannozzi, *Rev. Mod. Phys.*, 2001, **73**, 515–562.

